JAERI-M
92-008

STUDIES OF HIGH-LEVEL RADIOACTIVE WASTE FORM PERFORMANCE AT JAPAN ATOMIC ENERGY RESEARCH INSTITUTE

February 1992

Tsunetaka BANBA, Hiroshi KAMIZONO
and Hisayoshi MITAMURA

日本原子力研究所
Japan Atomic Energy Research Institute

JAERI-Mレポートは，日本原子力研究所が不定期に公刊している研究報告書です。
入手の問合わせは，日本原子力研究所技術情報部情報資料課（〒319－11茨城県那珂郡東海村）あて，お申しこしください。なお，このほかに財団法人原子力弘済会資料センター（〒319-11茨城県那珂郡東海村日本原子力研究所内）で複写による実費頒布をおこなっております。

JAERI-M reports are issued irregularly.
Inquiries about availability of the reports should be addressed to Information Division, Department of Technical Information. Japan Atomic Energy Research Institute, Tokai-mura, Naka-gun, Ibaraki-ken 319-11, Japan.

編集兼発行　日本原子力研究所
印　　刷　日立高速印刷株式会社

JAERI-M 92-008

Studies of High-level Radioactive Waste Form Performance at Japan Atomic Energy Research Institute

Tsunetaka BANBA, Hiroshi KAMIZONO and Hisayoshi MITAMURA

Department of Environmental Safety Research
Tokai Research Establishment
Japan Atomic Energy Research Institute
Tokai-mura, Naka-gun, Ibaraki-ken

(Received January 17, 1992)

The recent studies of high-level radioactive waste form at Japan Atomic Energy Research Institute can be classified into the following three categories;

(1) Study on the leaching behavior of the nuclear waste glass placing the focus on the alteration layer and the chemical composition of leachant for the prediction of the long-term corrosion of the waste glass.
(2) Study on the radiation (alpha-radiation) effects which have relation to the long-term stability of the nuclear waste glass.
(3) Study on the long-term self-irradiation damage of a SYNROC waste form using a curium-doped sample.

In the present report, the recent results corresponding to the above categories are described.

Keywords: Nuclear Waste Glass, Alteration Layer, Radiation Stability Leaching, Groundwater, Synroc, Density, Colloid, Swelling

---

This report was prepared for the first research coordination meeting of the IAEA Coordinated Research Programme (CRP) on "Performance of High-Level Waste Forms and Packages under Repository Conditions", which was held in KFK, Karlsruhe, Germany, from 11 to 15 November 1991.

原研における高レベル放射性廃棄物固化体に関する最近の研究成果

日本原子力研究所東海研究所環境安全研究部
馬場　恒孝・上薗　裕史・三田村久吉

（1992年1月17日受理）

原研における高レベル放射性廃棄物固化体に関する最近の研究は，次の3つに大別できる。

(1) ガラス固化体からの長期にわたる放射性核種漏洩量を予測するために必要な浸出挙動を，固化体表面に形成される変質層及び浸出液の化学組成の役割に注目して明らかにする研究。

(2) ガラス固化体の長期安定性に関係する照射による物性への影響（特にα崩壊による影響）に関する研究。

(3) キュリウム添加試料を使用したシンロック固化体の放射線損傷に関する研究。

本報告書では，それぞれに関係する最近の研究成果を報告する。

東海研究所：〒319－11　茨城県那珂郡東海村白方字白根2－4

なお，本報告書の内容は1991年11月，ドイツのカールスルーエ研究所で開催されたIAEA協力研究計画（CRP）「処分条件下の高レベル廃棄物固化体及び固化体容器の性能に関する研究調整会議」で発表したものをまとめたものである。

Contents

目　　次

1. Introduction

The Japan Atomic Energy Research Institute (JAERI) has contributed to the establishment of the national system for the high-level radioactive waste management with developments of safety assessment methods and accumulation of useful data. Besides, JAERI is responsible for researches of new technology to be acceptable to the Japanese environmental circumstances.

In the present document, the JAERI's studies on the properties of the nuclear waste glass and synroc are described briefly.

2. Growth Rate of Alteration Layer and Elemental Mass Losses during Leaching of Nuclear Waste Glass [1]

In order to validate the predictive models of the long-term corrosion of nuclear waste forms, the concept of natural analogues has been proposed [2]. The problem is, however, how we utilize the information of the natural analogues for modelling. One of the ways is to justify confidence in the theoretical model by correctly predicting the phases formed in the alteration layers of naturally and experimentally altered glasses. That is why a detailed understanding of the mineralogy and geochemistry of the layers is required [3]. In the present work, we will discuss on the growth rates of the alteration layers of a borosilicate nuclear waste glass and their relevance to elemental mass losses.

Experimental

MCC-1 leaching tests [4] were carried out for a borosilicate waste glass (Table 1) in deionized water for up to 364 days at 90°C. Four platy samples (0.2 × 0.5 × 0.5 cm) were put into a Teflon container for each leaching period. The surface area to solution volume ratio was 0.1 cm^{-1}. One of the four samples was immersed in ethanol for 2 hrs immediately after removing it from the leachate to prevent the shrinkage of the alteration layer during drying. The other samples were air-dried. Low viscosity epoxy resin was poured onto the ethanol-immersed sample when the ethanol was discarded. The air-dried samples were vacuum impregnated in the resin. After the polymerization of the resin, the samples were cut perpendicularly to the original glass surface and polished. The sections were subjected to optical micro-

1. Introduction

The Japan Atomic Energy Research Institute (JAERI) has contributed to the establishment of the national system for the high-level radioactive waste management with developments of safety assessment methods and accumulation of useful data. Besides, JAERI is responsible for researches of new technology to be acceptable to the Japanese environmental circumstances.

In the present document, the JAERI's studies on the properties of the nuclear waste glass and synroc are described briefly.

2. Growth Rate of Alteration Layer and Elemental Mass Losses during Leaching of Nuclear Waste Glass [1]

In order to validate the predictive models of the long-term corrosion of nuclear waste forms, the concept of natural analogues has been proposed [2]. The problem is, however, how we utilize the information of the natural analogues for modelling. One of the ways is to justify confidence in the theoretical model by correctly predicting the phases formed in the alteration layers of naturally and experimentally altered glasses. That is why a detailed understanding of the mineralogy and geochemistry of the layers is required [3]. In the present work, we will discuss on the growth rates of the alteration layers of a borosilicate nuclear waste glass and their relevance to elemental mass losses.

Experimental

MCC-1 leaching tests [4] were carried out for a borosilicate waste glass (Table 1) in deionized water for up to 364 days at 90°C. Four platy samples (0.2 × 0.5 × 0.5 cm) were put into a Teflon container for each leaching period. The surface area to solution volume ratio was 0.1 cm^{-1}. One of the four samples was immersed in ethanol for 2 hrs immediately after removing it from the leachate to prevent the shrinkage of the alteration layer during drying. The other samples were air-dried. Low viscosity epoxy resin was poured onto the ethanol-immersed sample when the ethanol was discarded. The air-dried samples were vacuum impregnated in the resin. After the polymerization of the resin, the samples were cut perpendicularly to the original glass surface and polished. The sections were subjected to optical micro-

scopy (OM) in order to measure the layer thicknesses. When the layers were too thin for OM, the samples were cut by ultramicrotomy, creating sections 50 to 80 nm thick, and then subjected to analytical electron microscopy (AEM). The sections were also observed by scanning electron microscopy (SEM) for texture examination. The concentrations of the major elements in the alteration layers were measured by electron microprobe analysis (EMPA). Fine structures and mass fractions of the alteration layers were examined by AEM. The solution pH was measured after leaching and the elemental concentrations of the leachates were measured by inductively coupled plasma atomic emission spectroscopy (ICP-AES) or atomic absorption spectrometry (AAS).

Results and discussion

There is a sharp change in the layer growth of the leaching experiments before and after 91 days (Fig. 1). The thickness of the layer increases linearly at a rate of 0.63 μm/day for up to 91 days. However, in the 91 to 364-day period, the thickness remains constant (about 60 μm). This suggests that significant corrosion of the glass almost ceases after the 91-day leaching. Grambow et al. [5] pointed out that on the basis of the time dependence of palagonite rind development, the range of values for the forward rate is 3-20 μm/1000yrs and the value for the final rate is 0.1 μm/1000yrs at about 3°C. The layer growth before the 91-day leaching corresponds to the corrosion of the forward reaction and the layer growth after the 91-day leaching, to the corrosion of the final reaction [6]. This is in good agreement with Si release data discussed below. We applied the relationship of the rates obtained by Grambow et al. [5] to our thickness measurements to calculate a corrosion rate of the final reaction of the waste glass. We assumed that the activation energy of the final reaction is the same as that of the forward reaction calculated from 3-20 μm/yr (3°C) and 0.63 μm/day (90°C), i.e. 89-107 kJ/mole. A range of values of 0.003-0.03 μm/day was obtained for the final rate. The layer thickness may increase by 0.9-9 μm for 300 days in the final reaction, which explains the small change in the thickness after the 91-day leaching (Fig. 1).

Figure 2 shows the normalized elemental mass losses of some typical elements. The apparent releases of B, Na and Si cease in the 91 to 364-day leaching period. The NLs of Na and Si are lower than that of B because Na and Si still remain in the layers (Table 3). Because the increase in layer thickness ceases after the 91-day leaching, B, Na, and Si are not supplied from the glass. It is reasonable to suggest that there is no significant

interactions, involving the three elements after 91 days.

The time dependence curves of B, Na and Si were similar to that of the layer thickness (Figs. 1 and 2), suggesting that the releases of these elements with time are related to the growth rate of the layer thickness. Because B can be completely depleted from the layer [7], the amounts of B in the leachates were used to calculate the layer thickness. The calculated values of layer thickness, represented by the triangles in Fig. 1, agreed well with the observed values from the OM or AEM measurements. It is thus confirmed that the alteration layer thickness can be estimated by the amounts of B released. The agreement also implies that the shrinkage of the alteration layers during air-drying is not significant.

The small shrinkage was also confirmed by comparing the thicknesses of the ethanol-immersed layers with those of the air-dried layers. The comparison has revealed that the air-dried layers had almost the same thicknesses as those of the ethanol-immersed layers in the 1 to 91-day leaching period, but were thinner by around 5 percent in the 91 to 364-day period (Fig. 1); the air-dried layers had larger variabilities in the thicknesses.

The small shrinkage suggests that the progressive change in the Fe mass fractions from 5.2 % in the glass/layer interface to 20.1 % in the layer/solution interface [3] does not result from shrinkage but from a real relative increase in the Fe fraction owing to the depletion of some elements such as Na, B and Si. This means that the layers are progressively more porous towards the layer/solution interface. The selected EMPA analyses (Table 3) also suggest the porous structure of the layer. For instance, in the outermost of the layer where crystalline fibers are scattered in the amorphous matrix [3], 70% of the original glass network formers are depleted (see the concentrations of B and Si in Tables 1 and 3). Thus, the alteration layer retains its structure despite the depletion of the large part of the glass network formers and the recrystallization. Naturally altered basaltic glasses are usually dried when they are obtained. It is not yet known whether the natural basaltic glass layers retain the structure of the layers after air-drying. The structural change of both naturally and experimentally altered layers during air-drying should be investigated.

The AEM studies revealed that new crystals have been formed in the 91-day experiment sample. The new crystals are texturally and chemically different from the fibers which are formed on the top of the layer [3]. The new crystals are distributed on the top of the fibers, and form a zonal structure like that of the fibers (Fig. 3). Both zones of the new crystals

and fibers are parallel to the pristine glass surface. The thicknesses of the fiber zone (denoted as 2 in Fig. 3a) are 120, 130, 120 and 220 nm in the 14, 28, 91 and 364-day experiment, respectively. Thus, the thicknesses of the fiber zone remain almost constant during the 91-day leaching of the glass. The fact that the fiber zone grows in the 91 to 364-day leaching period indicates that "the reaction at the final rate" [6] still continues. The thicknesses of the zone of the new crystals (denoted as 3 in Fig. 3a) are 440 and 480 nm in the 91 and 364-day experiments, respectively. The mass fractions of the fibers and mottled phase in the 364-day experiment (Table 2) have similar characteristics to those observed in the 14-day experiment [3]; rich in Fe, Mn, Co, and Ni, and none of the rare earth elements or Zr for the fibers, and rich in Fe, Zr, and the rare earch elements, and low in Co and Ni for the mottled phase. There appeared to be little change in the texture of the fibers and mottled phase near the layer/solution interface (Fig. 3a). The new crystals are characterized by the larger size (about 400 nm long), the consistent crystallographic orientation to the layer/solution interface (Fig. 3b), the d-spacing of 1.4 nm, and little Fe and enhanced Si (Table 2). These characteristics suggest that the new crystals are possibly smectite and therefore, mineralogically similar to the fibers. The mineralogical relationship between the new crystals and fibers is still under investigation. However, the thicknesses of the zones of the new crystals and fibers imply that the fibers grow while the new crystals do not and vice versa (e.g., 130 to 120 nm for the fiber zone and 0 to 440 nm for the new crystal zone in the 28 to 91-day leaching period).

The amount of Fe released in the solution is so small (Fig. 2) that it may be affected by the formation of minerals in the layer when Fe is not supplied from the glass, i.e., the layer thickness is almost constant. The growth of the fibers, which contain 10-18 % of Fe (Table 2, and Table II of ref. [3]), and the new crystals, which contain little Fe (Table 2), may account for the release of Fe in the solution: a slight decrease in the Fe release corresponds to the growth of the fibers and the non-growth of the new crystals in the 91 to 364-day leaching period.

Pit formation below the alteration layers was observed by OM and SEM on the samples leached for 91 to 364 days. Although the layer thickness ceased to increase, the degree of pitting increased with increase in the duration of the test. The cone-shaped pits (a few microns wide) are located inward from the glass-layer interface (Fig. 4). The loss of Na in the pit (number 2 in Table 3) indicates that the pits have been formed by the corrosion.

The composition of the pit is similar to that of the layer near the glass/layer interface (number 3 in Table 3). Harker and Flintoff have also observed similar pit formation and attributed the pitting phenomena to the physical structure in the glass such as stress lines, surface roughening and microcracks [8]. It is almost certain that the point of origin of every pit may be at a center of physical weakness such as microcracks. However, because the pits were not observed during the first 56 days of leaching, the pitting phenomena may be strongly dependent on the local chemistry of leach solution such as pH. Analogous phenomena were observed for naturally altered basaltic glasses by Melson and Thompson [9]. Pits, which they called microtubules, are a few microns wide and filled by clay minerals like smectite. Clay minerals formed following a 364-day leaching experiment have not yet been found in pits.

3. Leaching Behavior of High-Level Waste Glass in Synthetic Groundwater [10, 11]

The characteristics of groundwater affect leaching behavior of high-level waste glass, for example pH and Eh values may determine the precipitation processes of some elements in water. In the reduced synthetic groundwater which contains carbonate and sulfate ions, simulated high-level waste glass was subjected to static leach tests at 70° ± 1° and 20° ± 5°C. The glass-surface-area to leachant-volume ratio (SA/V ratio) was 0.24 cm^{-1} at 70°C and 0.12 cm^{-1} at 20°C. The static leach test at 70°C for up to 49 days was carried out in order to observe the process quickly. The static leach test at 20°C for 1 year was carried out for comparison with a former in-situ leach tests in one type of Japanese natural groundwater at 14°C. The four kinds of synthetic groundwater listed in Table 4 were used as leachants instead of the natural groundwater. Deionized water with a pH value of 5.6 and a specific resistance of 10^7 ohm cm was used as a reference.

Among normalized elemental mass losses (NL values) for the six elements, i.e., B, Si, Al, Fe, Nd and Ba, the value of NL_B was highest without exception, and the vaue of NL_{Ba} was lowest in some cases. The variation of NL_{Fe} is of particular interest, since it tended to be low in the case of deionized water and it was as high as NL_B in the case of synthetic groundwater Nos. 1 to 3 at 20°C. The ratio of NL_{Fe}/NL_B is introduced as an index expressing the extent of congruence. Table 5 summarizes the ratios of NL_{Fe}/NL_B under the

The composition of the pit is similar to that of the layer near the glass/layer interface (number 3 in Table 3). Harker and Flintoff have also observed similar pit formation and attributed the pitting phenomena to the physical structure in the glass such as stress lines, surface roughening and microcracks [8]. It is almost certain that the point of origin of every pit may be at a center of physical weakness such as microcracks. However, because the pits were not observed during the first 56 days of leaching, the pitting phenomena may be strongly dependent on the local chemistry of leach solution such as pH. Analogous phenomena were observed for naturally altered basaltic glasses by Melson and Thompson [9]. Pits, which they called microtubules, are a few microns wide and filled by clay minerals like smectite. Clay minerals formed following a 364-day leaching experiment have not yet been found in pits.

3. Leaching Behavior of High-Level Waste Glass in Synthetic Groundwater [10, 11]

The characteristics of groundwater affect leaching behavior of high-level waste glass, for example pH and Eh values may determine the precipitation processes of some elements in water. In the reduced synthetic groundwater which contains carbonate and sulfate ions, simulated high-level waste glass was subjected to static leach tests at 70° ± 1° and 20° ± 5°C. The glass-surface-area to leachant-volume ratio (SA/V ratio) was 0.24 cm^{-1} at 70°C and 0.12 cm^{-1} at 20°C. The static leach test at 70°C for up to 49 days was carried out in order to observe the process quickly. The static leach test at 20°C for 1 year was carried out for comparison with a former in-situ leach tests in one type of Japanese natural groundwater at 14°C. The four kinds of synthetic groundwater listed in Table 4 were used as leachants instead of the natural groundwater. Deionized water with a pH value of 5.6 and a specific resistance of 10^7 ohm cm was used as a reference.

Among normalized elemental mass losses (NL values) for the six elements, i.e., B, Si, Al, Fe, Nd and Ba, the value of NL_B was highest without exception, and the vaue of NL_{Ba} was lowest in some cases. The variation of NL_{Fe} is of particular interest, since it tended to be low in the case of deionized water and it was as high as NL_B in the case of synthetic groundwater Nos. 1 to 3 at 20°C. The ratio of NL_{Fe}/NL_B is introduced as an index expressing the extent of congruence. Table 5 summarizes the ratios of NL_{Fe}/NL_B under the

present experimental conditions. The results in Table 5 can be interpreted in two ways. First, the ratio in synthetic groundwater tends to be higher than that in deionized water for each temperature and time condition, which means that in synthetic groundwater iron tends to dissolve more congruently and not to precipitate on the glass surface during leaching. Second, when the kind of water is fixed, the ratios of NL_{Fe}/NL_B are ordered as: (20°C, 1 year) > (70°C, 28 days) > (70°C, 49 days) with the exception of synthetic groundwater No.4 where a slight variation occurs.

Grooves were observed on the surface of the specimens leached in synthetic groundwater Nos. 1 to 4. However, they were not clearly observed on the specimen leached in deionized water. It is thought that the grooves are clear in synthetic groundwater Nos. 1 to 4 when congruent leaching tends to occur and not clear in deionized water when incongruent leaching occurs. Such grooves were also observed on the surface of the specimens leached in natural groundwater.

In synthetic groundwater Nos. 1 to 4 which are reduced by tris-(hydroxymethyl)-aminomethane (THAM), the amount of Fe in the leachates increases as the Si increases probably as a result of the formation of $FeSiO_3$ colloidal particles or $FeSi_3O_3(OH)_8$ complex. It is not true that Fe very quickly reaches its saturation limit in synthetic groundwater Nos. 1 to 4, since the formation of the colloids or complex will increase the solubility of Fe in leachates. Because the filtration of the leachate at 20°C for 1 year through a 0.025 μm membrane had almost no effect on the concentrations of Fe and Si, $FeSiO_3$ colloidal particles, if present, have a diameter of less than 0.025 μm.

In deionized water in an oxidized condition, NL_{Fe}/NL_B was smaller than that of synthetic groundwater, but this is not because of the higher pH values of the leachates. For example, in deionized water at 20°C the pH value was 7.3 and smaller than that in synthetic groundwater. Even in deionized water, there is at least one example in which the solution concentration of Fe does not decrease as the pH value increases. This example was observed with leach experiments at a high SA/V ratio of 0.85 cm^{-1}.

The role of THAM should be mentioned here. It tends to increase the pH and to decrease the Eh of the solution. The pH values of the present synthetic groundwater were adjusted to 7.7 (Table 4), and for this purpose about 5 g of THAM were used for a 1 liter solution. The use of THAM is thought to be a major cause for the congruent dissolution of the glass in synthetic groundwater Nos. 1 to 4, since a Eh decrease by THAM in leachants will work effectively to form $FeSiO_3$ colloids or $FeSi_3O_3(OH)_8$ complex. As temperature

rises and as time proceeds, THAM as a reducing agent will be consumed with the progress of leaching, resulting in a lower NL_{Fe}/NL_B ratio.

In conclusion, the examination of the leaching behavior of high-level waste glass in synthetic groundwater is quite useful for identifying and understanding the mechanisms involved. Under somewhat reducing conditions, Fe dissolves easily into leachates, and hydrated silicate surface layer on the glass surface tends to dissolve more easily with Fe in reduced synthetic groundwater than in deionized water. In synthetic groundwater, cracks originally present on the glass tend to open and are observed as evidence of congruent glass corrosion. It is speculated that, in deep geologic disposal sites, congruent dissolution is more likely to occur in an reducing environment with a high SA/V-ratio.

4. Density Phenomena of an Actinide-Doped Borosilicate Waste Glass

The effects of annealing treatment on the density of an self-irradiated borosilicate waste glass were studied in the temperature range from 200°C to 500°C. The bulk composition of an actinide-doped glass sample is shown in Table 6. This glass contains 3.04 wt% curium-244 oxide and 0.96 wt% plutonium-238 oxide. The glass sample used for the experiment had a cumulative alpha dose of 1.7×10^{19} alpha decays/cm^3. This value is equivalent age of 1000,000 yrs for an actual waste glass. The densities of the glass specimens were measured by a sink-float method using two kinds of organic mixtures composed of 1-1-2-2-tetra-bromoethane and alpha-bromonaphtalene.

Figure 5 shows the density change during isochronal annealing for 1-hr at each temperature for irradiated samples. The density increases with an annealing temperature below 450°C. Conversely, above 450°C the density decreases sharply. This is probably because the annealing temperature approached the transition range of the waste glass. Under the isothermal annealing, the density increased rapidly during the initial 5 hours and approached to its equilibrium value at each temperature. As an example, the density change during isothermal annealing for irradiated specimens at 450°C is shown in Fig. 6.

The implications of these results were discussed using the model on the basis of the formation of helium bubbles in the glass and the recovery of network distortion. The density change of the irradiated glass during annealing due to the formation of helium bubbles is represented by the

rises and as time proceeds, THAM as a reducing agent will be consumed with the progress of leaching, resulting in a lower NL_{Fe}/NL_B ratio.

In conclusion, the examination of the leaching behavior of high-level waste glass in synthetic groundwater is quite useful for identifying and understanding the mechanisms involved. Under somewhat reducing conditions, Fe dissolves easily into leachates, and hydrated silicate surface layer on the glass surface tends to dissolve more easily with Fe in reduced synthetic groundwater than in deionized water. In synthetic groundwater, cracks originally present on the glass tend to open and are observed as evidence of congruent glass corrosion. It is speculated that, in deep geologic disposal sites, congruent dissolution is more likely to occur in an reducing environment with a high SA/V-ratio.

4. Density Phenomena of an Actinide-Doped Borosilicate Waste Glass

The effects of annealing treatment on the density of an self-irradiated borosilicate waste glass were studied in the temperature range from 200°C to 500°C. The bulk composition of an actinide-doped glass sample is shown in Table 6. This glass contains 3.04 wt% curium-244 oxide and 0.96 wt% plutonium-238 oxide. The glass sample used for the experiment had a cumulative alpha dose of 1.7×10^{19} alpha decays/cm^3. This value is equivalent age of 1000,000 yrs for an actual waste glass. The densities of the glass specimens were measured by a sink-float method using two kinds of organic mixtures composed of 1-1-2-2-tetra-bromoethane and alpha-bromonaphtalene.

Figure 5 shows the density change during isochronal annealing for 1-hr at each temperature for irradiated samples. The density increases with an annealing temperature below 450°C. Conversely, above 450°C the density decreases sharply. This is probably because the annealing temperature approached the transition range of the waste glass. Under the isothermal annealing, the density increased rapidly during the initial 5 hours and approached to its equilibrium value at each temperature. As an example, the density change during isothermal annealing for irradiated specimens at 450°C is shown in Fig. 6.

The implications of these results were discussed using the model on the basis of the formation of helium bubbles in the glass and the recovery of network distortion. The density change of the irradiated glass during annealing due to the formation of helium bubbles is represented by the

following equation.

$$\rho_{tr}(t) = \rho_0/\{1 + (4/3)\pi R(t)^3 N\} \qquad (1)$$

where $\rho_{tr}(t)$ is the density of the glass sample at the annealing time t, ρ_0 is the density of the unirradiated glass sample, R(t) is the radius of helium bubbles, and N is the number of helium bubbles per unit volume of glass sample, which is 1×10^{18} [bubbles/m^3] from our previous work [12]. Since the radius of helium bubble is $R(t) = [3k_BTm(t)/(8\pi\gamma)]^{1/2}$, R(t) can be calculated by using the surface tension of glass: $\gamma = 2$ J/m^3 [13], and the number of helium atoms in a bubble: m(t), which has been already obtained by our previous experimental work [14]. The calculated results at the annealing temperature of 450°C are represented by the dotted curve in Fig. 7.

On the other hand, the density change due to the recovery of glass network distortion is estimated by the following equation [15].

$$\rho_{dis}(t) = [1 + (\rho(\infty)/\rho_b - 1)(1 - \exp(-Bt))]\rho_b \qquad (2)$$

where $\rho_{dis}(t)$ is the density of the glass sample at the annealing time t, $\rho(\infty)$ is the density of the glass sample at $t = \infty$, ρ_b is the density of the glass sample at $t = 0$, and B is the constant on the distortion recovery. Fig. 7 shows the curves of density change calculated by the equation (1) (trapping model), by the equation (2) (distortion model), and by the summation of equation (1) and (2) (total) under the isothermal annealing at 450°C. Solid circles indicate the experimental data. As seen from this figure the experimental data agree well with the values calculated by the model including both the formation of helium bubbles in the glass and the recovery of network distortion.

5. Self-Irradiation Damage of a Curium-Doped Synroc Containing Sodium-Rich High-Level Nuclear Waste [16]

A polyphase titanate ceramic (synroc) immobilizing sodium-rich HLW was doped with 0.69 wt% of ^{244}Cm to accelerate long-term self-irradiation damage due to alpha decays. The composition of the curium-doped ceramic sample is shown in Table 7. Alpha autoradiography revealed a uniform distribution of the alpha-emitting nuclides on a >20μm scale, although micropores and

titanium oxide agglomerates were depleted in these nuclides. The curium-doped samples included sodium host phases such as freudenbergite and loveringite in addition to three main constituent minerals: hollandite, perovskite, and zirconolite. This phase assemblage was similar to a curium-free titanate ceramic. X-ray diffractometry on the annealed and as-damaged samples indicated that the alpha-emitting nuclides were incorporated into the actinide-host phases, perovskite and zirconolite, as the diffracted intensity of these phases was reduced in the latter samples.

Volume swelling due to accumulation of alpha decays caused a gradual decrease in density (Fig. 8). The increment of density after an equivalent age of 5000 yrs was -1%. Large volume swelling probably causes microcracking and an increase in surface area. Leach tests on 2000-yr samples showed significant increases in pH of leachate (Fig. 9) and leach rates of the soluble non-radioactive elements (Fig. 10, Fig. 11). Since sodium-rich HLW is likely to promote the formation of glassy phases leading to embrittlement of the waste form, chemical durability of the polyphase titanate ceramic against losses of soluble elements such as cesium may significantly decrease in unison with increasing alpha-decay damage. These damage effects must be further clarified by work which is continuing for longer equivalent ages. On the other hand, curium leach rates had a large scatter among data sets, although there was a slight trend to increasing the release rate with aging (Fig. 12). Since the present analytical method cannot distinguish between curium in true solution, in suspended or colloid forms, adsorbed on walls or as fine particles that might have been shed from the specimen surfaces, work is in progress to determine the contribution of leach forms of curium to the overall leach rate.

Acknowledgment

The authors wish to thank Dr. S. Muraoka for helpful suggestions and a critical reading of the manuscript.

titanium oxide agglomerates were depleted in these nuclides. The curium-doped samples included sodium host phases such as freudenbergite and loveringite in addition to three main constituent minerals: hollandite, perovskite, and zirconolite. This phase assemblage was similar to a curium-free titanate ceramic. X-ray diffractometry on the annealed and as-damaged samples indicated that the alpha-emitting nuclides were incorporated into the actinide-host phases, perovskite and zirconolite, as the diffracted intensity of these phases was reduced in the latter samples.

Volume swelling due to accumulation of alpha decays caused a gradual decrease in density (Fig. 8). The increment of density after an equivalent age of 5000 yrs was -1%. Large volume swelling probably causes microcracking and an increase in surface area. Leach tests on 2000-yr samples showed significant increases in pH of leachate (Fig. 9) and leach rates of the soluble non-radioactive elements (Fig. 10, Fig. 11). Since sodium-rich HLW is likely to promote the formation of glassy phases leading to embrittlement of the waste form, chemical durability of the polyphase titanate ceramic against losses of soluble elements such as cesium may significantly decrease in unison with increasing alpha-decay damage. These damage effects must be further clarified by work which is continuing for longer equivalent ages. On the other hand, curium leach rates had a large scatter among data sets, although there was a slight trend to increasing the release rate with aging (Fig. 12). Since the present analytical method cannot distinguish between curium in true solution, in suspended or colloid forms, adsorbed on walls or as fine particles that might have been shed from the specimen surfaces, work is in progress to determine the contribution of leach forms of curium to the overall leach rate.

Acknowledgment

The authors wish to thank Dr. S. Muraoka for helpful suggestions and a critical reading of the manuscript.

References

1) T. Banba, T. Murakami, and H. Isobe, in Scientific Basis for Nuclear Waste Management XIII, edited by V.M. Oversby and P.W. Brown (Materials Research Society, Pittsburgh, 1990), p.363.
2) R.C. Ewing and M.J. Jercinovic, in Scientific Basis for Nuclear Waste Management X, edited by J.K. Bates and W.B. Seefeldt (Materials Research Society, Pittsburgh, 1987), p.67.
3) T. Murakami, T. Banba, M.J. Jercinovic and R.C. Ewing, in Scientific Basis for Nuclear Waste Management XII, edited by W. Lutze and R.C. Ewing (Materials Research Society, Pittsburgh, 1989), p.65.
4) Materials Characterization Center, Nuclear Waste Materials Handbook, DOE/TIC-11400 (1981).
5) B. Grambow, M.J. Jercinovic, R.C. Ewing and C.D. Byers, in Scientific Basis for Nuclear Waste Management IX, edited by L.O. Werme (Materials Research Society, Pittsburgh, 1986), p.263.
6) B. Grambow, in Scientific Basis for Nuclear Waste Management VIII, edited by C.M. Jantzen, J.A. Stone and R.C. Ewing (Materials Research Society, Pittsburgh, 1985), p.15.
7) Zhihong Zhou and W.S. Fyfe, in Scientific Basis for Nuclear Waste Management XI, edited by M.J. Apted and R.E. Westerman (Materials Research Society, Pittsburgh, 1988), p.725.
8) A.B. Harker and J.F. Flintoff, Nucl. Technol., 76, 263 (1987).
9) W.G. Melson and G. Thompson, Geol. Soc. America Bull., 84, 703 (1973).
10) H. Kamizono, J. Nucl. Mater., 172, 319-324 (1990).
11) H. Kamizono, J. Mater. Sci. Lett., 9, 841-844 (1990).
12) S. Sato et al., J. Nucl. Mater., 152, 265 (1988).
13) J.F. DeNatale and D.G. Howitt, Nucl. Instr. and Meth., B1, 489 (1984).
14) H. Furuya et al., Proc. the first meeting on the JAERI/Universities co-operative program, p.87 (1990).
15) A.C. Damask, G.J. Dienes, Point Defects in Metals, Gordon and Breach, New York (1963).
16) H. Mitamura et al., J. Am. Ceram. Soc., 73, 3433 (1990).

Table 1 Bulk composition of the borosilicate waste glass.

Component	wt %	Component	wt %
Additives		FP oxides	
SiO_2	48.49	CoO	0.12[c]
B_2O_3	18.58	NiO	0.33[d]
Al_2O_3	2.00	TeO_2	0.23
Li_2O	1.87	Cs_2O	0.98
Na_2O	11.30	BaO	0.63
CaO	1.87	La_2O_3	0.51
Fe_2O_3	3.55[a]	CeO_2	1.42[e]
ZrO_2	2.87[b]	Pr_6O_{11}	0.50
		Nd_2O_3	1.65
FP oxides		Sm_2O_3	0.33
Rb_2O	0.12	Ag_2O	0.03
SrO	0.34	CdO	0.03
Y_2O_3	0.20	SnO_2	0.02
MoO_3	1.74	Sb_2O_3	0.004
MnO_2	0.26	Gd_2O_3	0.04

[a] Partly simulates RuO_2. [b] Partly includes ZrO_2 as FP.
[c] Simulates Rh_2O_3. [d] Simulates PdO.
[e] Partly simulates actinides.

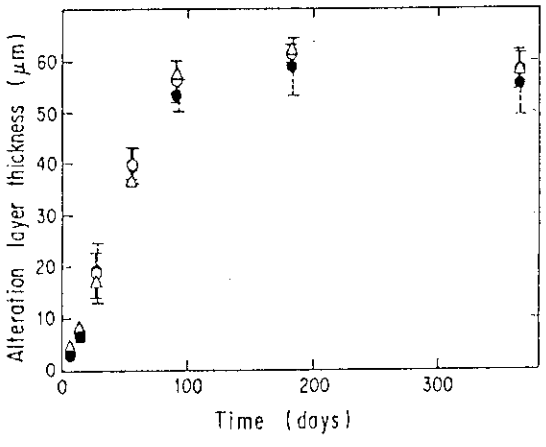

Fig. 1 Graph of the thickness of alteration layer as a function of leaching time under the MCC-1 conditions at 90°C. The open and solid circles indicate thicknesses averages for the ethanol-immersed and air-dried layers, respectively. The error bars represent the variabilities of the layer thicknesses. The triangles indicate layer thicknesses calculated from the amounts of B released in leachates.

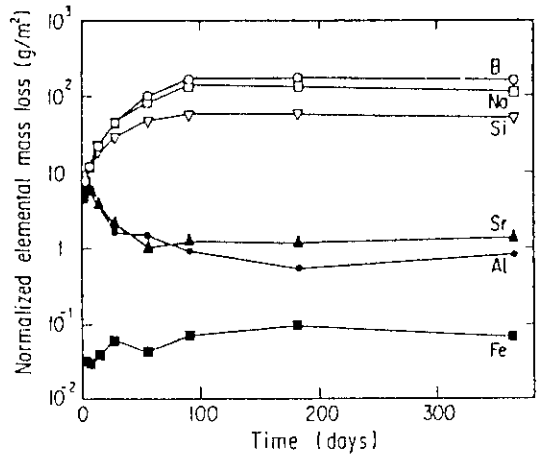

Fig. 2 Normalized elemental mass losses of selected elements of the nuclear waste glass in deionized water with time.

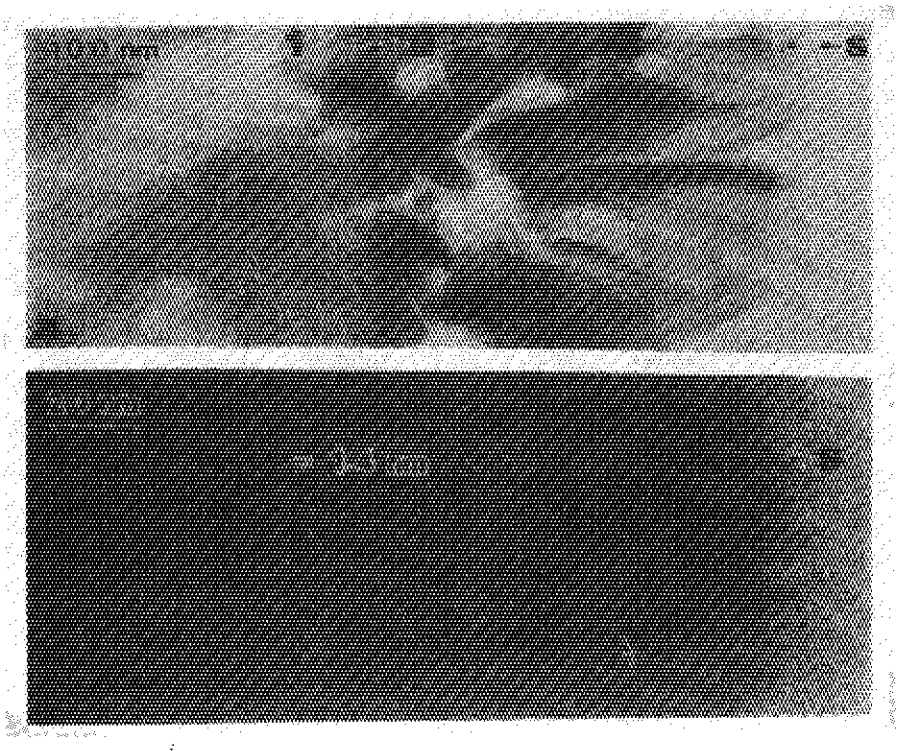

Fig. 3 TEM micrographs of the borosilicate glass layer. (a) Part of the layer in the 91-day experiment. 1 denotes the mottled phase in the layer [3] ; 2, the zone of the fibers formed on the layer; 3, the zone of the new crystals (possibly smectite); S, solution which is now filled with resin. The zones are parallel to the glass. The arrow indicates an example of the fibers in the mottled phase. (b) Part of the zone of the new crystals in the 364-day experiment. S shows the layer/solution interface. The d-spacings of the new crystals are mostly 1.4nm. Note that the c-axis, which is normal to the fringes, is parallel to the layer/solution interface or normal to the possible direction of cation diffusion. The arrow indicates an example of edge dislocation.

Table 2 AEM analyses of the new crystal (possibly smectite), fiber and mottled phase in the 364-day experiment (mass fraction, %).

	Na_2O	Al_2O_3	SiO_2	ZrO_2	CaO	MoO_3	MnO_2	FeO	CoO	NiO	REO[a]
New crystal	1.0	4.8	59.2	0.0	0.4	0.5	4.2	0.8	7.6	21.6	0.0
Fiber	1.5	8.5	49.2	0.0	0.6	0.5	4.3	10.6	5.5	19.3	0.0
Mottled[b]	1.5	3.4	55.4	10.6	1.7	0.4	1.9	10.9	0.6	2.0	11.7

[a] Sum of La_2O_3, CeO, and Nd_2O_3.
[b] See reference 3 for explanation of "mottled".

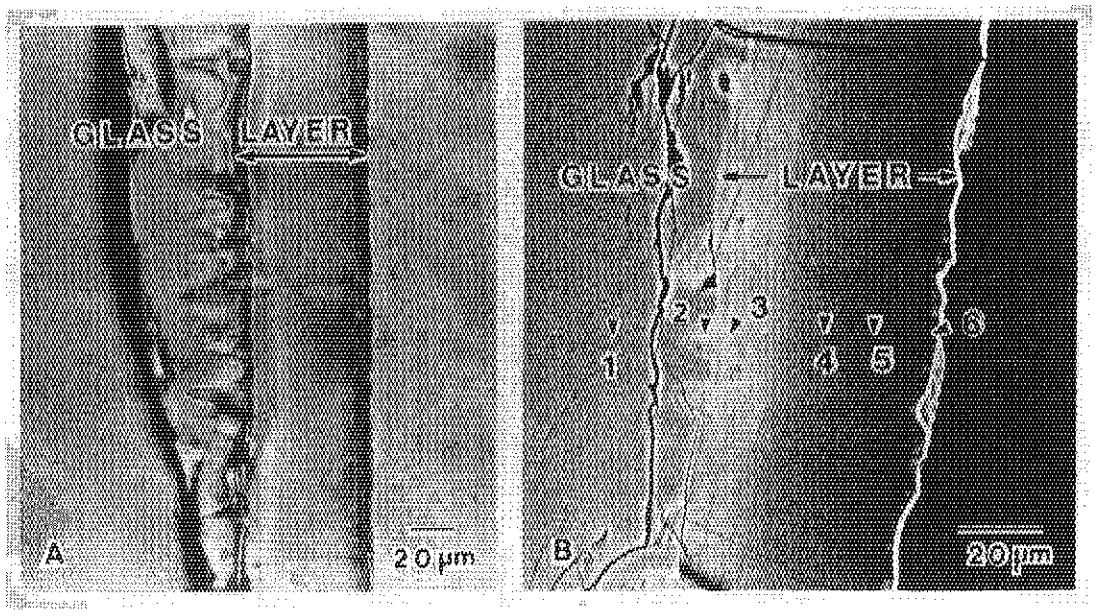

Fig. 4 Micrographs of the air-dried alteration layer in the 182-day experiment. (A) Optical view of the layer cross section showing cone-shaped pits. (B) SEM view (backscattered electron image) showing pits at the glass /layer interface. The locations of the six microprobe analyses are illustrated by the black arrowheads. The arabic numbers indicate the analytical points, corresponding to those in Table 3.

Table 3 Microprobe analyses (wt%)[a] of the glass and the alteration layer. The arabic numbers indicate the locations shown in Fig. 3B.

	Na_2O	Al_2O_3	SiO_2	CaO	MnO	FeO	Total
Bulk glass							
1	11.3	1.5	46.5	1.6	0.3	2.9	64.1
Layer							
2	2.2	2.5	50.4	5.4	0.4	3.8	64.7
3	1.5	2.5	51.1	4.2	0.3	4.2	63.8
4	1.4	3.1	42.9	2.2	-	3.9	53.5
5	1.7	2.8	37.0	2.1	0.4	3.7	47.7
6	-	1.5	29.3	1.6	0.7	3.6	36.7

[a] Obtained by Energy Dispersive X-ray (EDX) Analysis.

Table 4 Composition of synthetic groundwater

	Synthetic groundwater			
	No. 1	No. 2	No.3	No. 4
pH	7.7	7.7	7.7	7.7
Na (in mg/l) [a)]	26	26	26	26
Ca	120	120	–	–
Mg	108	108	108	–
HCO_3^-	Nearly saturated			
SO_4^{2-}	380	–	–	–

–: Not included.

[a)] The amount of each element in the synthetic groundwater is in the average concentration range of the respective element in the natural groundwater.

Table 5 The ratio of NL_{Fe}/NL_B in the leachates

Leach conditions	Synthetic groundwater				Deionized water
	No. 1	No. 2	No. 3	No. 4	
70°C, 28 days	0.35	0.36	0.66	0.24	0.0021
70°C, 49 days	0.13	0.24	0.20	0.51	0.0014
20°C, 1 year, not filtered	0.85	0.98	0.97	0.55	0.14
20°C, 1 year, filtered	1.02	0.82	1.01	0.59	0.16

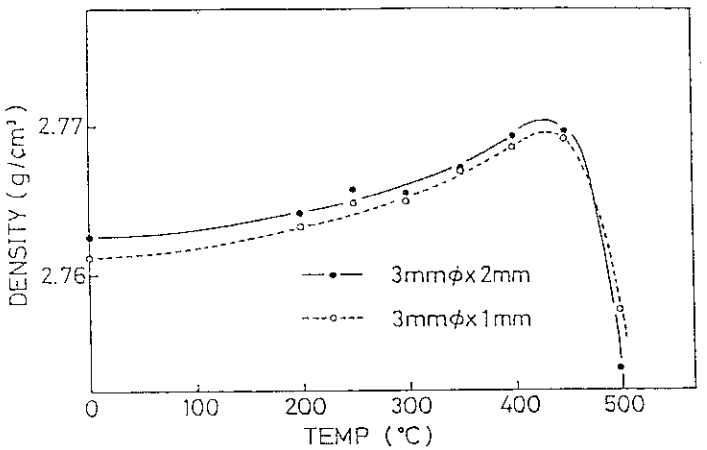

Fig. 5 Density change in isochronal annealing for 1 hour at each temperature for irradiated specimens.

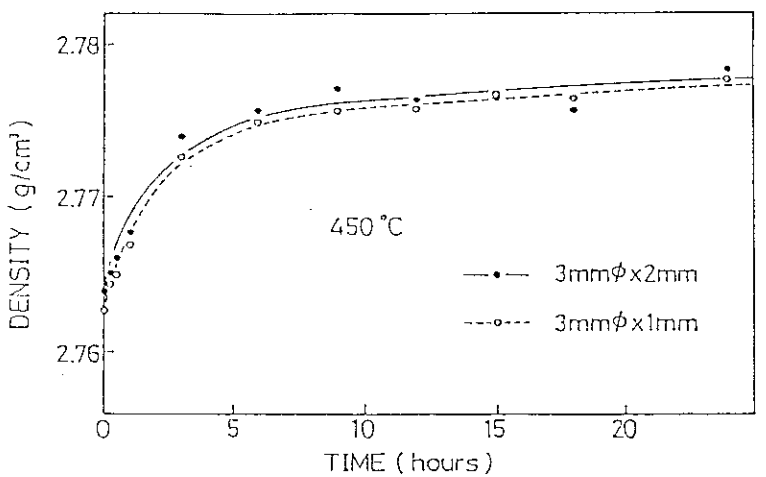

Fig. 6 Density change in isothermal annealing for irradiated specimens at 450°C.

Table 6 Bulk composition of an actinide-doped borosilicate waste glass.

Component	wt %	Component	wt %
Additives		Wastes	
SiO_2	45.15	Cs_2O	0.97
B_2O_3	13.90	BaO	0.62
Al_2O_3	4.89	La_2O_3	0.14
Li_2O	2.00	CeO_2	0.28
Na_2O	9.78[a]	Pr_6O_{11}	0.14
CaO	4.00	Nd_2O_3	0.45
ZnO	2.47	Sm_2O_3	0.09
		Eu_2O_3	0.02
Wastes		Gd_2O_3	0.01
Rb_2O	0.12	SeO_2	0.02
SrO	0.34	RuO_2	0.80
Y_2O_3	0.06	Fe_2O_3	2.90
ZrO_2	2.64[b]	NiO	0.40
MoO_3	1.73	Cr_2O_3	0.50
MnO_2	0.26	P_2O_5	0.30
Ag_2O	0.03	Ru	0.12
CdO	0.03	Rh	0.15
SnO_2	0.02	Pd	0.43
Sb_2O_3	0.01	Cm Oxides	3.04
TeO_2	0.23	Pu Oxides	0.96
		Total	100.00

[a] Partly contains Na_2O as chemicals added in the reprocessing.
[b] Partly contains ZrO_2 as zircalloy filings.

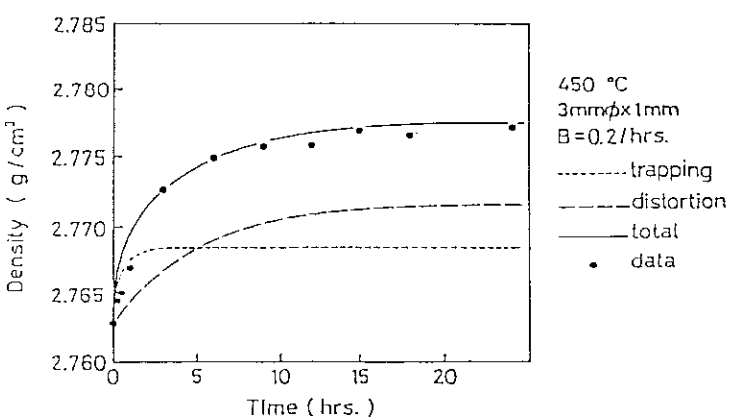

Fig. 7 The curves of density change calculated by the models based on the formation of helium bubbles in the glass (trapping model) and on the recovery of glass network distortion (distortion model) in isothermal annealing at 450°C. Solid circles show the experimental data.

Table 7 Nominal Composition of Curium-Doped Titanate Ceramic

Element	Content (wt%)
Precursor	
TiO_2	62.24
CaO	9.70
ZrO_2	5.95
BaO	4.81
Al_2O_3	4.72
Oxygen getter	
Ti (metal)	1.99
Simulated HLW	
ScO_2	0.011
Rb_2O	0.064
SrO	0.176
Y_2O_3	0.104
ZrO_2	0.852
MoO_3	0.899
MnO_2	0.133
RuO_2	0.506
Rh_2O_3	0.105
PdO	0.276
Ag_2O	0.015
CdO	0.016
SnO_2	0.010
Sb_2O_3	0.002
TeO_2	0.118
Cs_2O	0.507
BaO	0.325
La_2O_3	0.263
CeO_2	0.524
Pr_6O_{11}	0.257
Nd_2O_3	0.237
$CmO_2 + PuO_2$	1.614
Na_2O	1.652
P_2O_5	0.167
Fe_2O_3	1.382
Cr_2O_3	0.200
NiO	0.175

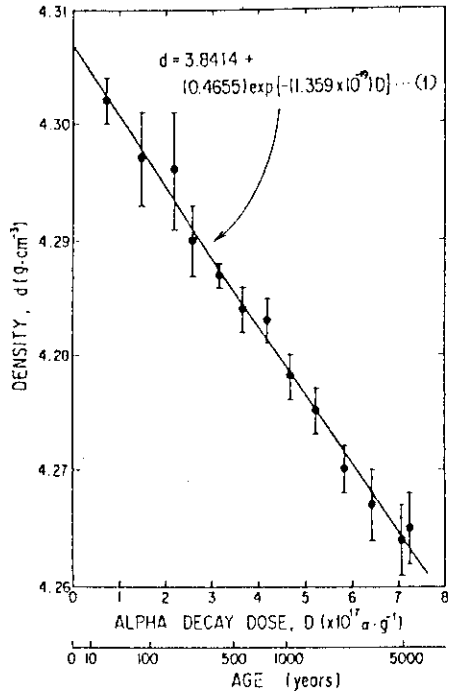

Fig. 8 Density of curium-doped titanate ceramic versus α-decay dose. Equivalent age corresponding to an α-decay dose is also shown. Solid line is derived from fitting by use of Eq (1).

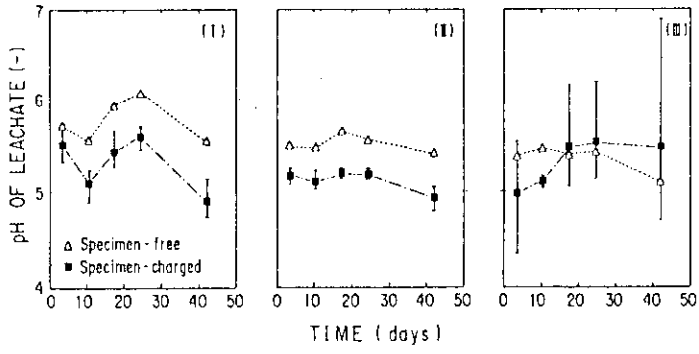

Fig. 9 Change in pH of leachate from curium-doped titanate ceramic versus leach time. (I), (II), and (III) correspond to equivalent ages of 130, 330, and 2000yr, respectively. Error bars attached to the average indicate the largest and smallest values among three sets of specimen-charged data in each run. In (I), displacement in time is probably due to a pH calibration problem.

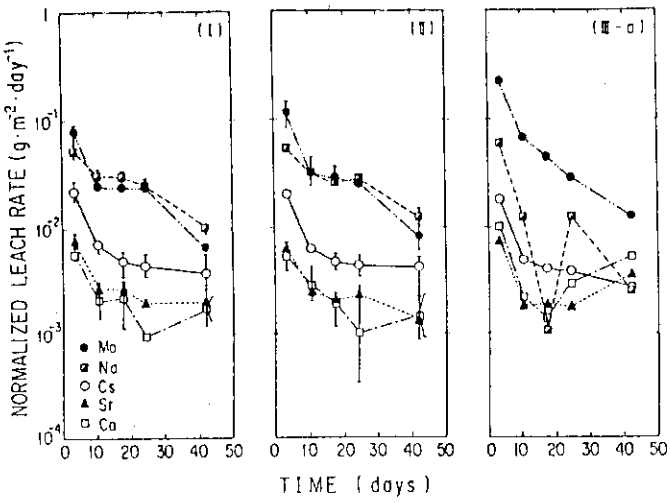

Fig. 10 Comparison of normalized leach rates of nonradioactive elements from curium-doped titanate ceramic of different ages. (I),(II), and (III-a) correspond to equivalent ages of 130, 330, and 2000yr, respectively. Error bars attached to the average in (I) and (II) indicate the largest and smallest values among three sets of data in each run. (III-a) shows the data obtained from a single half-disk among three 2000-yr specimens.

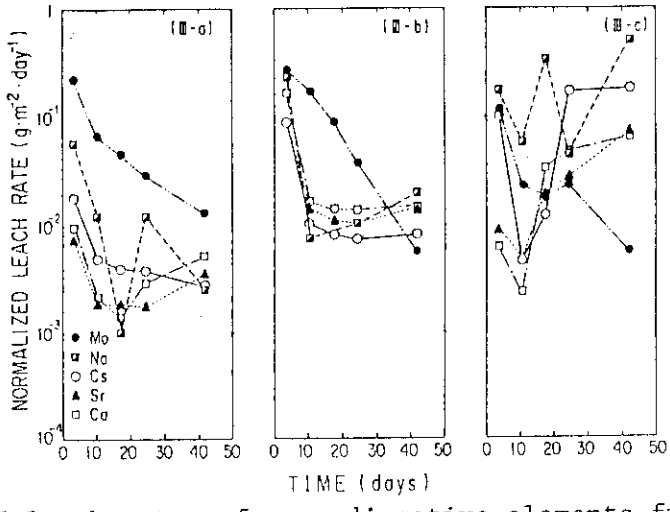

Fig. 11 Normalized leach rates of nonradioactive elements from three different 2000-yr specimens of curium-doped titanate ceramic.

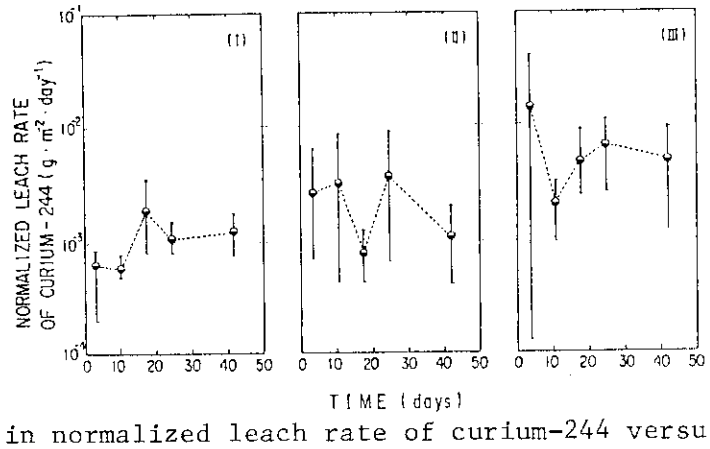

Fig. 12 Change in normalized leach rate of curium-244 versus leach time. (I), (II) and (III) correspond to equivalent ages of 130, 330, and 2000yr, respectively. Error bars attached to the average indicate the largest and smallest values among three sets of data in each run.